Earth and Space Science

RESEARCH ARTICLE
10.1029/2023EA003167

Alfvén-Fast Wave Coupling in a 2D Nonuniform Medium

R. Davies[1] and **A. N. Wright**[1]

[1]School of Mathematics and Statistics, University of St Andrews, St Andrews, UK

Key Points:

- Alfvén-fast mode conversion is relevant for magnetospheric Alfvén waves of multiple planets such as Jupiter and the Earth
- Alfvén waves are surprisingly efficient at transmitting energy through an inhomogeneity, for both increases and decreases of Alfvén speed
- The transmitted energy of waves which experience mode coupling does not change monotonically with the magnitude of the nonuniformity

Supporting Information:

Supporting Information may be found in the online version of this article.

Correspondence to:

R. Davies and A. N. Wright,
rd203@st-andrews.ac.uk;
anw@st-andrews.ac.uk

Citation:

Davies, R., & Wright, A. N. (2023). Alfvén-fast wave coupling in a 2D nonuniform medium. *Earth and Space Science*, *10*, e2023EA003167. https://doi.org/10.1029/2023EA003167

Received 12 JUL 2023
Accepted 22 SEP 2023

Author Contributions:

Conceptualization: A. N. Wright
Investigation: R. Davies
Supervision: A. N. Wright
Writing – original draft: R. Davies
Writing – review & editing: A. N. Wright

Abstract A 2D Cartesian simulation is presented and used to solve the ideal, low-beta, linear magnetohydrodynamics equations. A simulation is used to investigate the propagation of Alfvén waves through inhomogeneities in Alfvén speed and density. In particular, the loss of Alfvén wave energy through coupling to the fast wave, and also the form of the Alfvén wave as it emerges from the inhomogeneous region is studied. Potential applications of this include the magnetospheres of both Jupiter and the Earth. The results show that Alfvén waves can be significantly distorted by a nonuniformity and still propagate through the region efficiently, with relatively small amounts of Alfvén wave energy lost through mode conversion and reflection.

Plain Language Summary Many objects are surrounded by magnetic fields for example, the Earth and the Sun. Just as waves travel in water or sound waves travel through the air, some types of waves can travel through magnetic fields, these waves have lots of roles, including producing the aurora or Northern Lights. In this paper, computer simulation is used to investigate the conversion of one type of wave (the Alfvén wave) into a second type of wave (the fast magneto-acoustic wave), through a process called wave mode coupling, which occurs when the magnetic Alfvén wave travels through a region where its speed changes. The results show that even when the Alfvén wave is significantly distorted by the change in speed it is still able to carry a high percentage of its energy through. One situation this might be important in is increasing the understanding of Alfvén waves at Jupiter, created by the moon Io, which interact with Jupiter's aurora.

1. Introduction

The existence of magnetohydrodynamic (MHD) waves, in both the solar and planetary magnetospheres, is well documented (Nakariakov et al., 2016; Wright, 1987; Yates et al., 2016). In uniform mediums the three MHD wave modes: fast, Alfvén, and slow, are independent; however, nonuniform mediums produce waves with "mixed properties" (Goossens et al., 2019); this process is known as "wave mode conversion" or "wave mode coupling." A specific instance of mode coupling is fast-Alfvén conversion. This occurs in the solar corona through the process of resonant absorption (Rae & Roberts, 1982), which has been suggested as a contributing process in coronal heating (Erdélyi, 2007; Ofman et al., 1994). Cally and Goossens (2008) show, through three-dimensional simulation, that the production of Alfvén waves through resonant absorption is highly dependent on the angle between the Alfvén wave vector and the magnetic field lines. In planetary magnetospheres, it has been shown that fast waves can drive Alfvén waves through the process of field line resonance (Southwood, 1974). This has wide reaching implications for the transfer of energy and momentum throughout the magnetosphere, taking energy from global to local scales (see review by Elsden et al., 2022).

This paper focuses on the opposite process, Alfvén-fast coupling. The coupling of Alfvén waves propagating near to magnetic X-lines (a simple model for magnetic reconnection) in a linear, low-beta plasma, to the fast mode was first investigated by Bulanov et al. (1992). This work was later extended by McClements et al. (2006), who suggested that this process may be significant in coronal heating. The nonlinear coupling of Alfvén and fast waves in regions where Alfvén phase mixing occurs was considered by Nakariakov et al. (1997), who focused on the generated fast wave and its potential applications in coronal MHD. Zheng et al. (2015) found strong dependence on the plasma beta, and that a longer scale length of the density inhomogeneity produced higher amplitude fast waves, corroborating the result of Botha et al. (2000). Boocock and Tsiklauri (2022) compared linear and nonlinear models of torsional Alfvén wave propagation through open structures in the solar corona, finding that Alfvén-fast wave coupling occurred due to nonlinear effects. The effect of nonuniform mediums on Alfvén wave propagation has also been studied extensively from the point of view of reflection and transmission (Soler et al., 2017).

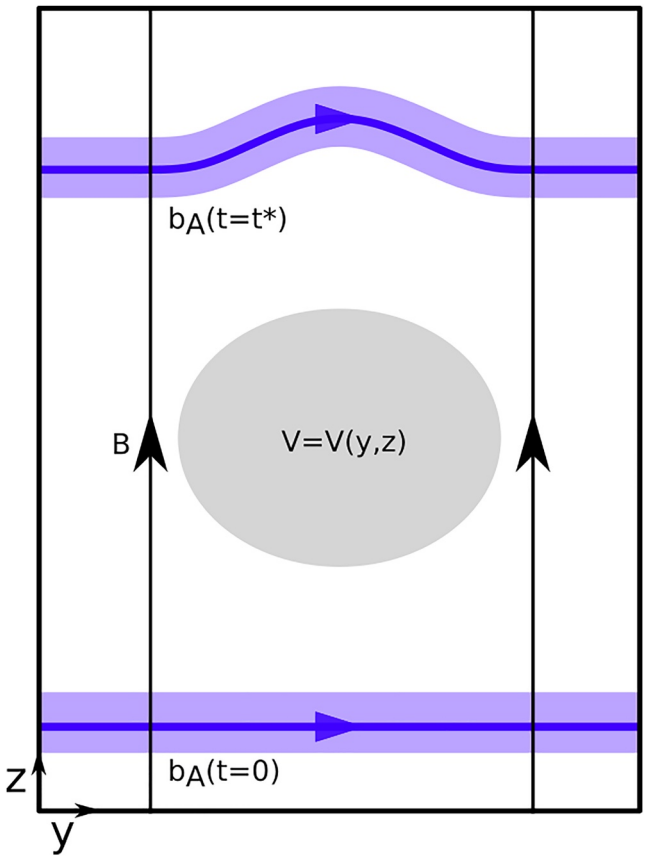

Figure 1. A diagram illustrating the propagation of an Alfvén wave pulse through a nonuniformity in the WKB limit, for a cold plasma. The location of the Alfvén wave pulse is shown by the regions of blue shading. The solid blue lines mark the location of the wave peak, with the arrowhead indicating the direction of the perturbation magnetic field. The gray shading indicates a nonuniform region for the case where the Alfvén speed is increased, elsewhere the Alfvén speed is uniform. The Alfvén wave is shown for $t = 0$, where the wave is invariant in y, and $t = t^*$, after the Alfvén wave has propagated through the nonuniform region, with the central part of the wave having propagated further than the edges, due to the nonuniform region where V increases. This leads to the conclusion that b_A must have a field-aligned component and the wave, therefore, cannot be purely Alfvén.

In this paper, Alfvén-fast wave coupling, caused by nonuniform Alfvén speed, is investigated in ideal, linear, low-beta MHD, using numerical modeling in two dimensions. This process may occur in the Earth's magnetosphere. Alfvén waves are involved in many processes in the different regions of the magnetosphere, such as field line resonance; energy transport during substorms, in the plasma sheet boundary layer; and Pi2-associated Alfvén waves, in the plasmasphere (Keiling, 2009). As these waves propagate from the magneto-tail to the ionosphere, through several pronounced density gradients, it is likely that Alfvén-fast wave coupling will occur. This process may also be relevant to the formation of Alfvén wave ducts, which has been shown using global geospace simulations (Yang et al., 2022). Alfvén ducts are field-aligned channels that allow efficient transmission of Alfvénic energy due to their relatively uniform and low Alfvén wave conductance.

Alfvén-fast wave coupling may also occur in other planetary magnetospheres. One example of this is the interaction of the moon Io with the Jovian magnetosphere which drives Alfvén waves in the Io-Jupiter flux tube. These waves propagate through significant changes in Alfvén speed between the dense Io plasma torus and the less dense plasma outside of it (Wright, 1987). The Alfvén wave driven by Io interacts with Jupiter's ionosphere, creating a bright spot in the aurora at the foot point of the flux tube (Mura et al., 2018). This interaction is not unique to Io. Ganymede also produces an auroral bright spot (Grodent et al., 2009), and a bright point can be observed in Saturn's aurora associated with the moon Enceladus (Pryor et al., 2011). The fact that Alfvén waves are able to maintain their identity to such a high degree when propagating in a nonuniform medium is surprising, and provides the motivation for the simulations presented here.

The simplest thought experiment that can encapsulate the coupling of an Alfvén wave to other wave modes is illustrated in a 2D low plasma beta system in Figure 1, which shows a section of an infinite medium that is permeated by a uniform background magnetic field, **B**, which is aligned with the z coordinate. The Alfvén speed, V, is uniform everywhere except for the region shaded gray, where it increases. The bottom of the figure shows an Alfvén wave pulse and the associated perturbation magnetic field, b_A. Here, the shaded blue region represents the location of the wave pulse, with the darker line and arrow representing the location of the peak of the wave and the direction of the perturbation magnetic field. The Alfvén wave propagates along the background field and encounters the region of increased Alfvén speed. What is the effect on the Alfvén wave of trying to propagate through this region?

A naive interpretation could be based on WKB (Wentzel–Kramers–Brillouin) theory, where reflection is neglected and it is assumed that the whole wave is transmitted through the nonuniform section and simply travels at the local Alfvén speed. The result would look something similar to the Alfvén wave shown at the top of Figure 1, where the parts of the wave which encountered the higher V region have run ahead of the parts of the wave that did not. However, there is evidently a problem with this picture: there are sections of the b_A field line that have a component parallel to **B**, so the wave has generated a compressional ($b_\parallel$) component. As a cold, low-beta plasma is considered; this cannot be part of an Alfvén wave, which must have $b_\parallel = 0$. The generation of $b_\parallel$ indicates the presence of the fast mode. Hence, this simple thought experiment leads to the conclusion that when an Alfvén wave propagates through a suitable nonuniform medium it will couple to the fast mode, even in the WKB approximation. This conclusion raises many questions such as how much of the initial Alfvén wave energy is lost to the fast mode? How much energy is transmitted as an Alfvén wave? What is the spatial structure of the transmitted Alfvén wave? How have the field-aligned currents (important for particle acceleration) been affected? This paper makes a start at answering some of these questions through the use of numerical simulation.

The paper is structured as follows: Section 2 discusses the numerical model, including the governing equations, system equilibrium, and step sizes. Section 3 presents the results of the investigation, with the nonuniform region having either an increasing or decreasing Alfvén speed profile. (The increasing case is considered for two different spatial extents in z.) Section 4 discusses the conclusions that can be drawn from the investigation and gives some final remarks.

2. Model and Governing Equations

2.1. Governing Equations

The simulation uses a two-dimensional Cartesian coordinate system (y, z) and the ideal, low-beta, linear MHD equations. The equations are normalized by the following quantities: magnetic field strength, B_0, the magnetic field strength at the origin; speeds, V_0, the Alfvén speed at the origin; distances, L_0, the simulation width in y; density, ρ_0, the density at the origin; and time, $T_0 = L_0/V_0$. The normalized equations are:

$$\frac{\partial u_y}{\partial t} = \frac{B}{\rho}\left(\frac{\partial b_y}{\partial z} - \frac{\partial b_z}{\partial y}\right) \tag{1}$$

$$\frac{\partial b_y}{\partial t} = B\frac{\partial u_y}{\partial z} \tag{2}$$

$$\frac{\partial b_z}{\partial t} = -B\left(\frac{\partial u_y}{\partial y}\right) \tag{3}$$

$$\mathbf{B} = B\,\hat{\mathbf{z}} \tag{4}$$

$$\rho = \rho(y, z) \tag{5}$$

With u_y, b_y, b_z the perturbations of the velocity and magnetic field; B, the background magnetic field strength; and ρ, the density. The background magnetic field, $\mathbf{B}$, is uniform and parallel to the z-axis. It should be noted that the normalizing factors are the values at the origin. Hence, B_0, the normalizing factor, and B, the normalized background field strength, are distinct quantities. Equations 1–3 are the component forms of the momentum and induction equations in the (y, z) coordinate system, such that $\partial/\partial x = 0$ and $u_x = b_x = 0$, with the chosen background magnetic field.

2.2. Computational Grids and Boundary Conditions

A system of staggered grids, with constant spacing Δy, Δz, are used to store the perturbation fields u_y, b_y, b_z. $\mathbf{G_{0,0}}$ is the grid which the origin lies on. $\mathbf{G_{1,0}}$ is the grid, transposed by $\Delta y/2$ in the y-axis. Similarly $\mathbf{G_{0,1}}$ is transposed by $\Delta z/2$ in the z-axis and $\mathbf{G_{1,1}}$ is transposed in both axes. u_y is stored on $\mathbf{G_{1,0}}$. b_y is stored on $\mathbf{G_{1,1}}$ and b_z is stored on $\mathbf{G_{0,0}}$. This means that b_z is known on all boundaries, however, u_y and b_y are known only on the boundaries in the z- and y-axes, respectively. The choice of grids was made to allow central differencing to calculate the derivatives in Equations 1–3 on the correct grids. For example, in Equation 1, the required derivatives are $\partial b_y/\partial z$ and $\partial b_z/\partial y$, which will lie on the same grid as u_y.

The boundary conditions are periodic in both axes. In the y-axis, this means that the simulation domain could be considered as a closed loop, like a flux tube at a constant radial value. The choice of a periodic boundary in the z-axis is not significant as the extent in z is chosen with respect to the run time, so that no perturbations encounter these boundaries.

2.3. Nonuniform Alfvén Speed Profile

The nonuniform nature of the simulation is imposed by defining an Alfvén speed profile, on which the density is dependent, as $\rho(y, z) = B^2/V(y, z)^2$. The Alfvén speed is uniform, with background value V_{bg} everywhere outside of an isolated nonuniform region, $y_a < y < y_b$, $z_a < z < z_b$. The Alfvén speed profile is smooth and continuous, with a single maximum or minimum. The difference between the maximum or minimum, $\tilde{V}$, and the background

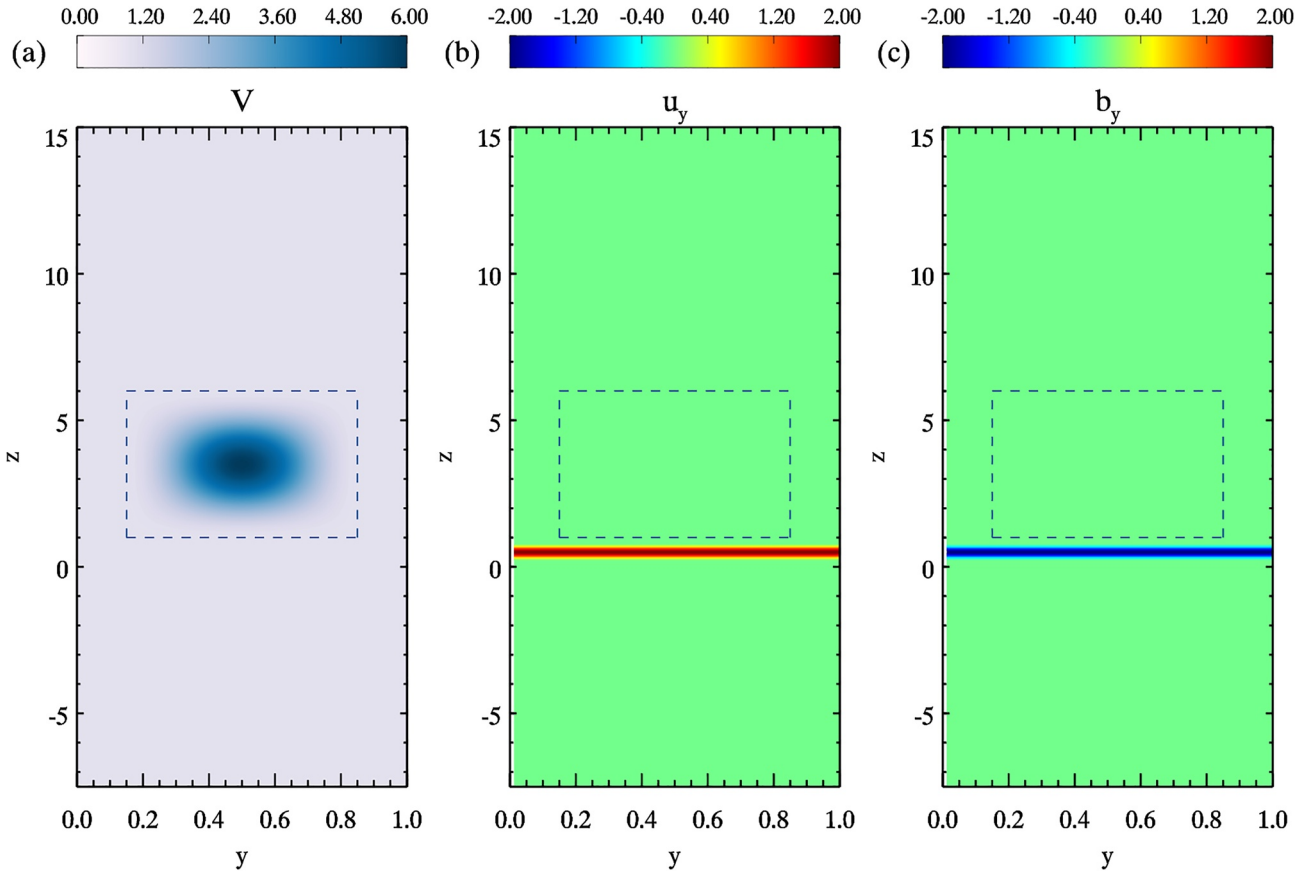

Figure 2. Contour plots of the Alfvén speed profile and wave initialization. Panel (a) shows an example of the Alfvén speed profile for the case where $\Delta V = 5$. The plot shows the geometry of the Alfvén speed profile with two uniform regions of the simulation domain $z < z_a = 1$ and $z > z_b = 6$. The nonuniformity is contained in the region, $y_a = 0.15 < y < y_b = 0.85$, $z_a = 1 < z < z_b = 6$, this is marked on all three plots by the dashed rectangle. Panels (b and c) show the initialization of the Alfvén wave, at $t = 0$, in the lower uniform region with perturbations of velocity and magnetic field in the y direction, u_y, and b_y. The wave pulse is defined analytically and is nonzero in the region $0.2 < z < 0.8$ and is invariant in y.

Alfvén speed, V_{bg}, is denoted ΔV, with $\Delta V = \tilde{V} - V_{bg}$, therefore, ΔV is positive if the Alfvén speed increases and negative if the Alfvén speed decreases in the nonuniform region.

The Alfvén speed profile is given by:

$$V(y,z) = \begin{cases} 1 + \frac{\Delta V}{4}\left(1 - \cos\left(2\pi \frac{z - z_a}{z_b - z_a}\right)\right)\left(1 - \cos\left(2\pi \frac{y - y_a}{y_b - y_a}\right)\right), & y_a < y < y_b, \\ & z_a < z < z_b, \\ 1, & \text{elsewhere} \end{cases} \quad (6)$$

where $y_a = 0.15$, $y_b = 0.85$. In the standard cases, Sections 3.1 and 3.2, $z_a = 1$, $z_b = 6$, therefore, the maximum or minimum will lie at $y = 0.5$, $z = 3.5$. This is illustrated in Figure 2a for $\Delta V = 5$. In the extended nonuniformity case, Section 3.3, $z_a = 1$, $z_b = 11$, therefore, the maximum or minimum will lie at $y = 0.5$, $z = 6$.

2.4. Initial Configuration

The simulation is initialized analytically, in the lower uniform region, with an Alfvén pulse centered at $z = 0.5$, with no dependence on y, propagating in the positive z-direction. The Alfvén wave is defined by:

$$u_y = f(\chi) \quad (7)$$

$$b_y = -\rho^{\frac{1}{2}} f(\chi) \tag{8}$$

with

$$f(\chi) = \begin{cases} 1 - \cos\left(2\pi \frac{\chi - 0.2}{0.6}\right), & 0.2 < \chi < 0.8 \\ 0, & \text{elsewhere} \end{cases} \tag{9}$$

where $\chi = z - Vt$.

Contour plots of the initial u_y and b_y are shown in Figures 2b and 2c. From the initialization position, the Alfvén wave propagates (in the z-direction) at the background Alfvén speed until it reaches the lower boundary of the nonuniformity, $z_a = 1$. As the wave propagates through the nonuniformity it couples to the fast mode and takes on mixed properties. The wave modes decouple as the wave propagates into the upper uniform region, $z_b > 6$. The extent of the nonuniform region in z, $z_b - z_a$, is chosen to be large relative to the width of the Alfvén pulse in z, which minimizes reflection off the nonuniformity, as the investigation focus is the effect of wave coupling (rather than reflection) on the Alfvén wave.

2.5. Numerical Details

The simulation uses the second order Leapfrog-Trapezoidal scheme (Zalesak, 1979) for the numerical integration of the governing equations, with the boundary conditions applied to both the predictor and corrector steps of the algorithm. Δt is chosen to satisfy the CFL condition and give an acceptable error.

Test runs of the simulation show good energy conservation for $(\Delta y, \Delta z) = (0.025, 0.00625)$, with Δt dependent on ΔV, such that Δt decreases where ΔV increases. The choice of Δt gives energy conversation of 99.93% or better. It improves when ΔV becomes large as the time-step is reduced for the whole domain, though the propagation speed between grid points only increases within the nonuniform region. The simulation requires higher resolution in z than in y, due to the difference in the length scales of the wave in each direction.

2.6. Wave Mode Separation

In a uniform medium, the fast and Alfvén wave modes are not coupled, therefore, the total perturbations can be separated into fast and Alfvén parts, such that $\mathbf{u} = \mathbf{u_A} + \mathbf{u_F}$, and similarly for $\mathbf{b}$. As the simulation has periodic boundary conditions in y, at a fixed z, z^*, the perturbation fields along this line, $u_y(y, z^*)$, $b_y(y, z^*)$, and $b_z(y, z^*)$ can each be decomposed into a Fourier sum. Alfvén waves are incompressible, therefore, $\partial u_{Ay}/\partial y = 0$. It follows that $u_{Ay}(y, z^*)$ will be equal to the 0th term in the Fourier sum, and all higher-order terms will form $u_{Fy}(y, z^*)$. The same will be true for $b_y(y, z^*)$.

$$u_y(y, z^*) = \underbrace{\frac{a_0}{2}}_{\text{Alfvén}} + \underbrace{\sum_{n=1}^{\infty} (a_n \cos(ny) + b_n \sin(ny))}_{\text{Fast}} \tag{10}$$

$$= u_{Ay} + u_{Fy} \tag{11}$$

$$b_y(y, z^*) = \underbrace{\frac{c_0}{2}}_{\text{Alfvén}} + \underbrace{\sum_{n=1}^{\infty} (c_n \cos(ny) + d_n \sin(ny))}_{\text{Fast}} \tag{12}$$

$$= b_{Ay} + b_{Fy} \tag{13}$$

The compressional magnetic field $b_z(y, z^*)$ is entirely associated with the fast mode and has no 0th Fourier term.

$$b_z(y, z^*) = \underbrace{0}_{\text{Alfvén}} + \underbrace{\sum_{n=1}^{\infty} (e_n \cos(ny) + f_n \sin(ny))}_{\text{Fast}} \tag{14}$$

$$= b_{Fz} \tag{15}$$

3. Results and Discussion

The code is used to investigate two related cases, $\Delta V > 0$ and $\Delta V < 0$, where the nonuniformity is bounded by $z_a = 1$, $z_b = 6$. For the $\Delta V > 0$ case, a run time of 12.5 time units is chosen, with the simulation bounded in z by $z = -12$ and $z = 20$, which will ensure the wave does not encounter these boundaries. The run time and simulation domain are extended to 25 time units and $-24 < z < 26$ for the $\Delta V < 0$ case to account for the slowing of the wave in the nonuniform region and to allow wave energy to escape the nonuniformity. A third case is also considered, where the ΔV is positive ($\Delta V > 0$) case is revisited, with the geometry of the nonuniform region modified such that the extent of the nonuniform region in z is doubled. The new nonuniform region is bounded by $z_a = 1$, $z_b = 11$. To account for this, the duration of the simulation is extended from 12.5 to 17.5 time units, and the simulation is bounded by $-17 < z < 28$.

3.1. $\Delta V > 0$ Case

Figure 3 shows the location of the wave at three time-steps of the simulation, for $\Delta V = 5$. The nonuniformity is marked on each panel by the dashed rectangle which marks the boundaries $y_a = 0.15$, $y_b = 0.85$, $z_a = 1$, $z_b = 6$. Figures 3a–3c, show the initial configuration of the Alfvén wave at $t = 0$, which is invariant in y and is in a region of uniform Alfvén speed. It is clear from Figure 3c that there is no b_z, this is expected as b_z is associated only with the fast mode, which should not be present. Figures 3d–3f show the wave at $t = 3.75$, as it propagates through the nonuniformity. Figures 3d, u_y, and 3e, b_y, show that the wave becomes distorted inside the dashed rectangle and the clear invariance in y is lost. In Figure 3f, b_z is clearly nonzero, demonstrating that mode coupling is occurring. These Figures 3d–3f also show that there is some reflection of the wave off the nonuniformity at $t = 3.75$. Figures 3g–3i show the wave at $t = 12.5$, the simulation end time, in the upper uniform region, $z > z_b = 6$. In Figures 3g, u_y, and 3h, b_y the invariance in y has been recovered by the leading parts of the wave, this transitions into a sinusoidal pattern for the trailing parts of the wave. This sinusoidal behavior is also seen in the same area of Figure 3i for the b_z component. These distinct patterns allow the different wave modes to be visually identified, the y invariant perturbations are Alfvénic, and the sinusoidal perturbations are fast.

To analyze the behavior of the individual fast and Alfvén waves, the total perturbations outputted by the simulation, u_y, b_y, and b_z, were decomposed (as described in Section 2.6) to produce two new sets of variables: u_{Ay}, b_{Ay}, b_{Az} and u_{Fy}, b_{Fy}, b_{Fz}. These variables are valid for $z < z_a = 1$ and $z > z_b = 6$, where the Alfvén speed is uniform. As the Alfvén wave has no b_z component, $b_{Az} = 0$, $b_{Fz} = b_z$.

The total energy per unit length in x within the simulation, E, can be divided into the Alfvén energy, E_A, and the fast energy, E_F. These quantities are given by:

$$E = \frac{1}{2}\int \rho u_y^2 + b_y^2 + b_z^2 \, dy dz \tag{16}$$

$$E_A = \frac{1}{2}\int \rho u_{Ay}^2 + b_{Ay}^2 \, dy dz \tag{17}$$

$$E_F = \frac{1}{2}\int \rho u_{Fy}^2 + b_{Fy}^2 + b_z^2 \, dy dz \tag{18}$$

Since the Alfvén and fast modes are orthogonal $E = E_A + E_F$ (when considering a domain in z where the medium is uniform). Similarly the energy density in z (and unit length in x) can be found by integrating in y. The corresponding total energy density, $\mathcal{E}$, and those for the Alfvén, $\mathcal{E}_A$, and fast, $\mathcal{E}_F$, wave energy density are:

$$\mathcal{E}(z) = \frac{1}{2}\int \rho u_y(y,z)^2 + b_y(y,z)^2 + b_z(y,z)^2 \, dy \tag{19}$$

$$\mathcal{E}_A(z) = \frac{1}{2}\int \rho u_{Ay}(y,z)^2 + b_{Ay}(y,z)^2 \, dy \tag{20}$$

10.1029/2023EA003167

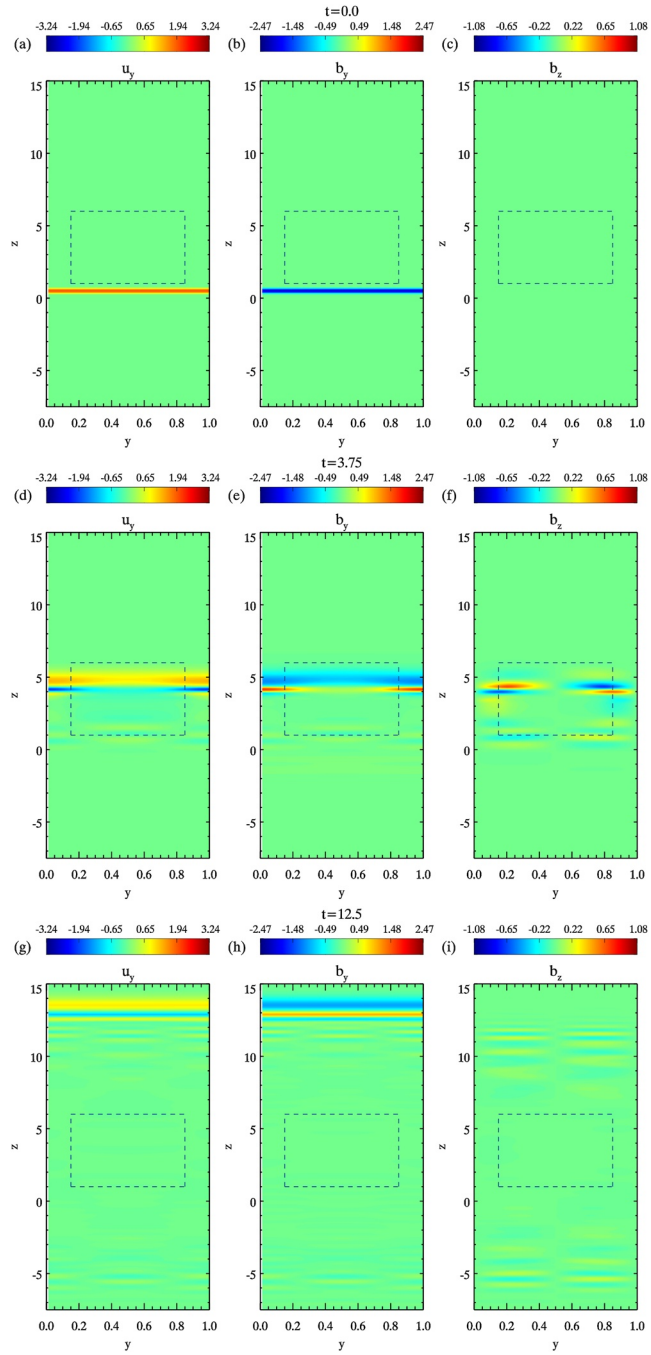

Figure 3. Contour plots of the simulation perturbations, $\Delta V = 5$. Each row of contour plots show u_y, b_y, and b_z at a particular time, for $\Delta V = 5$. The over-plotted dashed rectangles mark the region where the Alfvén speed is non-uniform. Panels (a–c) show the wave at $t = 0.0$. The wave is in the lower uniform region of the simulation, therefore, there has been no mode coupling, and there is no b_z. Panels (d–f) show the wave at $t = 3.75$, propagating through the nonuniform region (marked by the dashed rectangle), and the wave has mixed properties. There are clear contributions in b_z. Panels (g–i) show the wave at $t = 12.5$, the end of the simulation. The transmitted waves are now in the upper uniform region and the reflected waves in the lower. Evidence of both wave modes can be seen in panels (g and h). The parts of the wave that have propagated furthest ($z > 13.5$) appear invariant in y are associated with the Alfvén wave. The waves that have a sinusoidal y variation (also visible in panel (i)) are compressional and come from the fast mode. The movie from which these snapshots are taken is included in the Supporting Information S1.

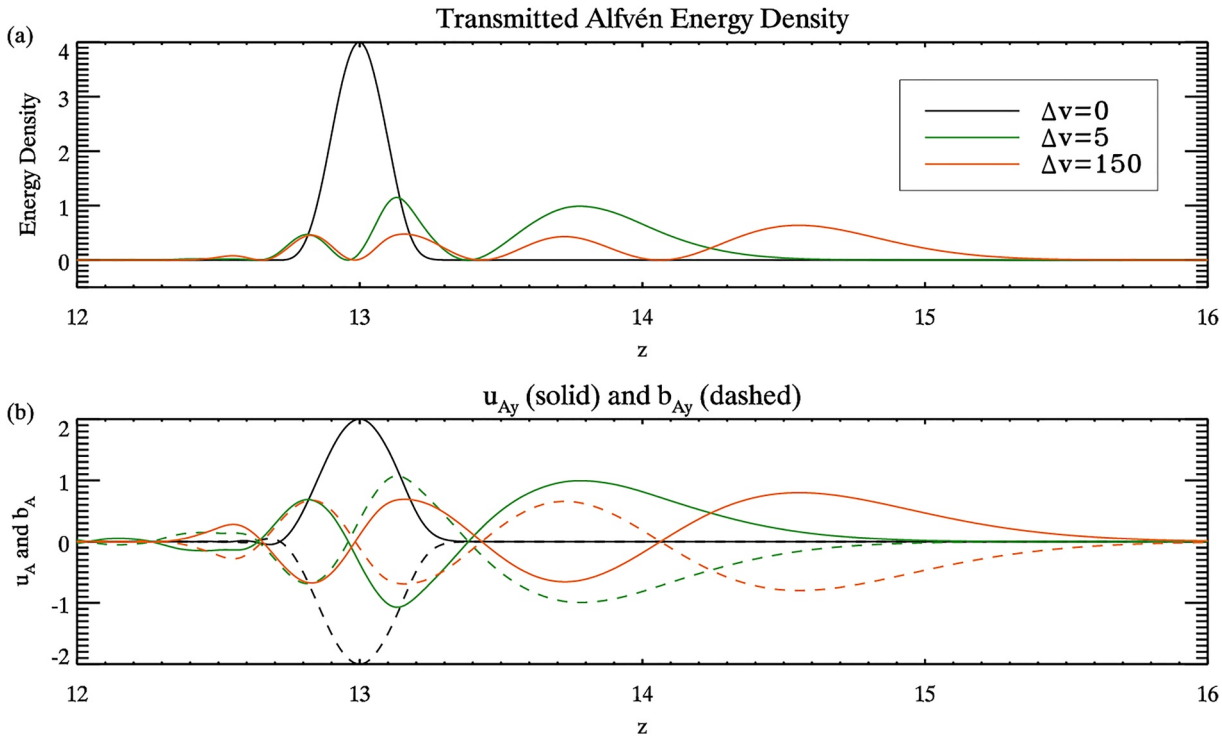

Figure 4. Transmitted Alfvén energy density (in z) and transmitted Alfvén wave perturbations, for $t = 12.5$, $\Delta V > 0$. Panel (a) shows the energy density in z of the transmitted Alfvén wave, $\mathcal{E}_A$ (see Equation 20), in the region $12 < z < 16$ at the simulation end time, $t = 12.5$. Panel (b) shows the Alfvén wave perturbations u_{Ay} and b_{Ay} which correspond to the lines in panel (a) and clearly satisfy $\rho^{1/2}u_y = -b_y$ ($\rho = 1$ for $z > z_b = 6$). Both panels show the stretching of the Alfvén wave created by propagation through the nonuniformity, which has caused the wave to develop multiple peaks and increased the width of the leading peak.

$$\mathcal{E}_F(z) = \frac{1}{2}\int \rho u_{Fy}(y,z)^2 + b_{Fy}(y,z)^2 + b_z(y,z)^2\, dy \tag{21}$$

To produce Figure 4, the Alfvén energy density, $\mathcal{E}_A$, was calculated for each slice of the simulation in z (in the transmitted region, $z > z_b = 6$), at the simulation's final time, $t = 12.5$, using Equation 20. The black line, $\Delta V = 0$, is a translation of the initial Alfvén energy having perfectly maintained its structure as the medium is uniform and no wave coupling occurred. The green line, $\Delta V = 5$, shows significant distortion of the Alfvén wave profile in the direction of propagation, with three peaks of lower amplitude. The leading edge of the wave has propagated significantly further, approximately 1.4 units of length, compared to the $\Delta V = 0$ (black line) case. The orange line, $\Delta V = 150$, clearly displays the continuation of these trends, with an additional peak and reduced peak amplitudes. The leading edge of this wave propagates 2.2 length units ahead of the $\Delta V = 0$ case.

The maximum possible propagation distance of the leading edge of the Alfvén wave can be calculated from the propagation time through the center ($y = 0.5$) of the nonuniform region in the z-direction, $T_p = \int_1^6 1/V(0.5, z)\, dz$, the background Alfvén speed and the original position of the leading edge ($z = 0.8$). As the simulation runs for a fixed length of time (12.5 normalized time units), it is clear that the sum of the propagation time of the leading edge through each region of the domain must be 12.5, such that $12.5 = T_{u1} + T_p + T_{u2}$, where $T_{u1} = 0.2$, the time taken to travel the initial distance between the leading edge of the wave and the start of the nonuniformity; T_p, as defined above, is the minimum propagation time through the nonuniformity; and T_{u2} is the time the leading edge of the wave is propagating in the upper uniform region. As the Alfvén wave is propagating in the uniform region ($z > z_b = 6$, where $V = V_{bg} = 1$) for a time T_{u2}, the maximum possible z it can reach by the end of the simulation is Z_{max}, where $Z_{max} = z_b + VT_{u2} = 6 + T_{u2}$. Using this to eliminate T_{u2} in the previous relation gives, $Z_{max} = 18.3 - T_p$.

For the $\Delta V = 0$ case, this gives $Z_{max} = 13.3$, in good agreement with the leading edge of the black line in Figure 4. $\Delta V = 5$ gives $Z_{max} = 16.2$, yet the leading edge of the green line is at $Z_{sim} \approx 14.8$. The discrepancy is even greater for the $\Delta V = 150$ case as $Z_{max} = 17.9$, yet the orange line suggests that the Alfvén wave has only reached $Z_{sim} \approx 15.7$. Clearly the leading edge of the Alfvén wave does not propagate at the maximum possible Alfvén

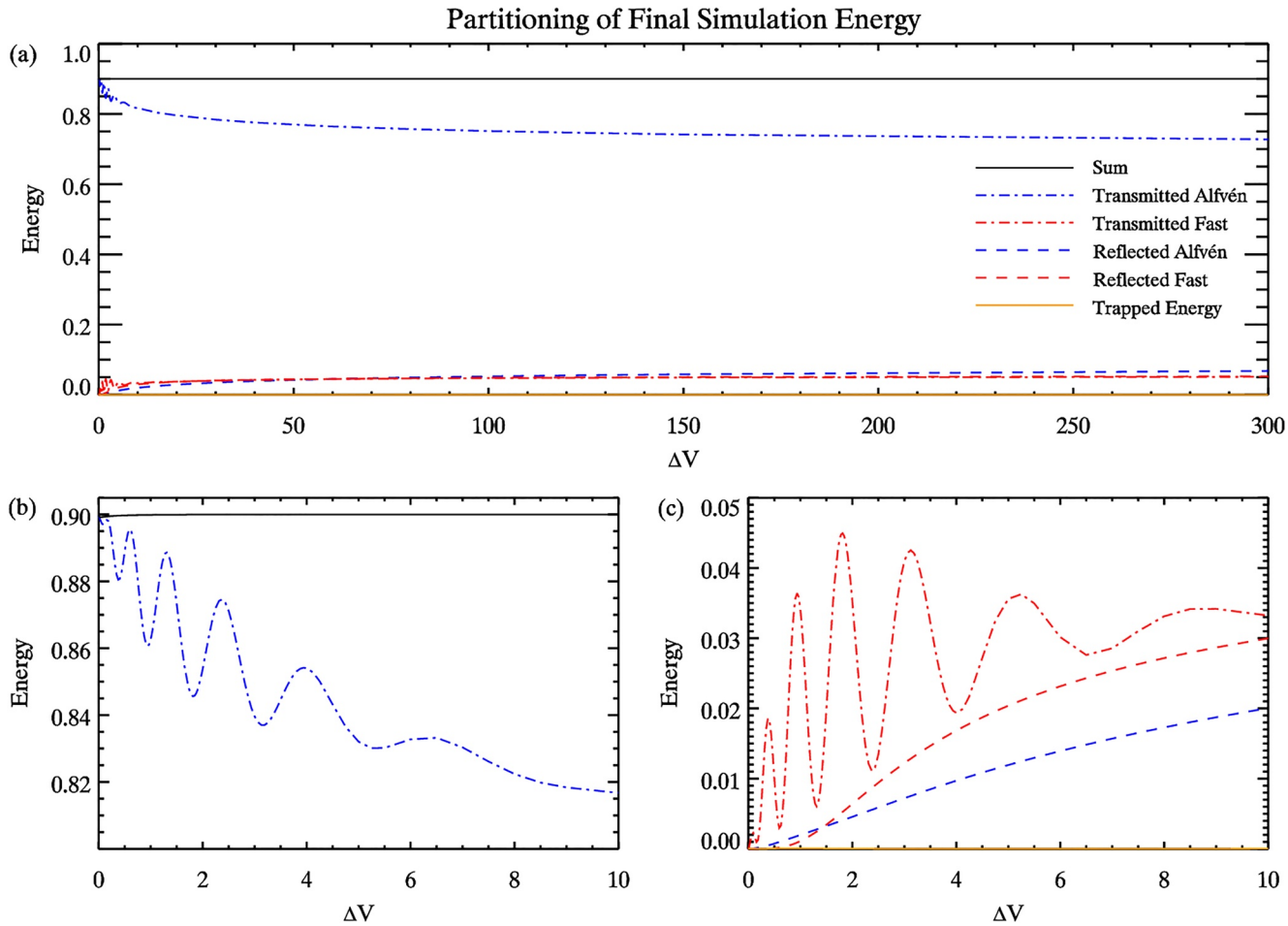

Figure 5. Partitioning of simulation energy between different waves. These plots show how the energy associated with the transmitted and reflected waves at the simulation end time changes with ΔV. All panels show the same data set. Panel (a) shows all wave categories for the range $0 < \Delta V < 300$. It can be seen that all energies quickly asymptote, with the most interesting behavior occurring in $0 < \Delta V < 10$. Panels (b and c) show a close-up of the region $0 < \Delta V < 10$, with the larger energies shown in panel (b) and the smaller quantities in panel (c). Interesting oscillatory behavior is seen in both of the transmitted waves, but is not present in the reflections. The wave energy trapped in the nonuniform region is clearly negligible.

speed. This is not too surprising. Evidently, the parts of the wave that propagate in the lower V regions (particularly $y < y_a = 0.15$ and $y > y_b = 0.85$, where $V = V_{bg} = 1$) play a crucial role and hold back the Alfvén wave as a whole. The range in z over which the transmitted wave resides is clearly a complicated function of V. The effective time at which the nonuniform region is traversed lies between the maximum and the minimum transit times. It should also be noted that the nonuniformity causes the Alfvén wave to broaden its spatial scale significantly.

Figure 5 was created using 70 runs of the simulation, for values of ΔV spanning the range 0–300. For each of these runs data was collected from the simulation end point, $t = 12.5$. Transmitted energy is taken to be the energy of the perturbations in the upper uniform region, $z > z_b = 6$, and reflected energy in the lower uniform region, $z < z_a = 1$. Using Equations 17 and 18 with the appropriate limits, the transmitted and reflected energy associated with each wave mode can be calculated. For the transmitted Alfvén wave, this is simply the energy under the curves in Figure 4. Energy trapped in the nonuniform region was calculated using the total perturbations (see Equation 16) in $1 < z < 6$.

Figure 5a shows the entire range $0 < \Delta V < 300$, with the transmitted Alfvén energy appearing to decrease as ΔV increases and quickly starting to asymptote to 0.725. The values for the transmitted fast, reflected fast, and reflected Alfvén energy are largely similar, beginning to diverge slightly for $\Delta V > 150$, they are significantly smaller than the transmitted Alfvén energy for all values of ΔV. The trapped energy is clearly negligible, with a maximum value of 8.6×10^{-4}.

Figures 5b and 5c show a much smaller range in the horizontal axis $0 < \Delta V < 10$, and smaller ranges in the vertical axis, with Figure 5b showing the transmitted Alfvén energy and the total energy; and Figure 5c showing the smaller quantities. Figure 5c shows that the most fast energy is generated when $\Delta V \approx 1.47$ or $\Delta V \approx 3.13$. Figures 5b and 5c show interesting behavior of the transmitted waves, which rather than being monotonic, display oscillatory behavior as ΔV increases. This behavior is not seen in the reflected waves. The oscillations are well resolved. When compared with a run at double the resolution, the difference between the high and standard resolution transmitted Alfvén energy was 4×10^{-4}, while the amplitude of the oscillations in the transmitted Alfvén wave energy is approximately 2×10^{-2}.

3.2. $\Delta V < 0$ Case

Figure 6 shows the location of the wave for three snapshots of the simulation, where $\Delta V = -0.3$, that is, where the normalized Alfvén speed decreases from the background value of 1 to a minimum value of 0.7. It appears that any reflection off the nonuniformity is minimal as this is not visible on the contour plots. The reflection would be visible in Figures 6d–6f, though it would propagate out of the region shown in Figures 6g–6i. There are clear contributions in b_z, in panel (f), showing the presence of the fast mode. In panels (g)–(i), where the wave has propagated into the upper uniform region, evidence of both wave modes can be seen on the contour plots, as in the $\Delta V = 5$ case. Again, the furthest propagating parts of the wave which are invariant in y, and dominate the u_y and b_y contour plots in panels (g) and (h) are Alfvénic, and the fainter, sinusoidal patterned waves visible in all three panels are fast.

To produce Figure 7, the simulation variables were again decomposed, as described in Section 2.6 to produce two new sets of variables associated with the Alfvén wave (u_{Ay}, b_{Ay}, b_{Az}) and the fast wave (u_{Fy}, b_{Fy}, b_{Fz}). The simulation total, Alfvén and fast energies and energy densities in z were found using Equations 16–18 and 19–21.

In Figure 7, as in Figure 4, the $\Delta V = 0$ black line is a translation of the initial condition in z by the simulation run time (since $V = 1$). In this subsection, the run time is 25.0 time units, so the peak should be centered on $z = 25.5$. The green lines, $\Delta V = -0.3$, show that the wave is slowed down and stretched by the nonuniform region, and the single peak of the initial condition becomes three peaks with decreasing amplitudes. The spatial scale of the first peak has also increased significantly. The orange line, $\Delta V = -0.9$, shows the same features, but with the wave having been affected much more intensely. In panel (a), there are five clear peaks with decreasing spatial scale. The peak amplitudes reach a maximum at peak three, located at $z = 14.9$.

The calculation of the predicted location for the $\Delta V > 0$ case in Section 3.1 can be repeated for this case, with small modifications to account for the change in run time and setup. In this case, as part of the wave is slowed down, it is clearer to consider the location of the trailing edge of the wave, rather than the leading edge, as some parts of the wave do not encounter the nonuniformity and are not slowed down. In this subsection, $25.0 = T_{u1} + T_p + T_{u2}$, as the simulation run time is increased to 25.0 units, where T_{u1} is the time taken for the trailing edge of the wave to propagate up to the nonuniform region; T_p is the time for the trailing edge of the wave to propagate through the nonuniform region and T_{u2} is the time the trailing edge of the wave propagates in the upper uniform region for. Recall that in this subsection ($\Delta V < 0$), the position of the trailing edge of the wave pulse is considered rather than the leading edge. Therefore, T_{u1} will change such that $T_{u1} = 0.8$, as the initial position of the trailing edge of the wave pulse is $z = 0.2$. The formula for T_p will be unchanged $\left(T_p = \int_1^6 1/V(0.5, z)\, dz\right)$ but its value is dependent on $V = V(y, z)$ which is in turn dependent on ΔV. T_{u2} is related to $Z_{\min}$, the minimum possible position of the trailing edge in z at the simulation end time, by $Z_{\min} = z_b + VT_{u2}$. Recalling that $z_b = 6$, $V = 1$ in the upper uniform region and substituting for T_{u2} it is found that $Z_{\min} = 30.2 - T_p$.

For the $\Delta V = 0$ case, shown by the black line in Figure 7, this gives $Z_{\min} = 25.2$, which matches the simulation result. For $\Delta V = -0.3$, shown by the green line, $Z_{\min} = 24.2$ which is almost exactly where the trailing edge of the wave pulse is seen in the plot. $\Delta V = -0.9$ gives $Z_{\min} = 14.4$, which is slightly ahead of where the trailing edge is seen on the plot; this is likely due to some of the wave being briefly trapped in the nonuniform region and making a delayed exit. It is interesting that these predictions are much more accurate in the $\Delta V < 0$ regime.

10.1029/2023EA003167

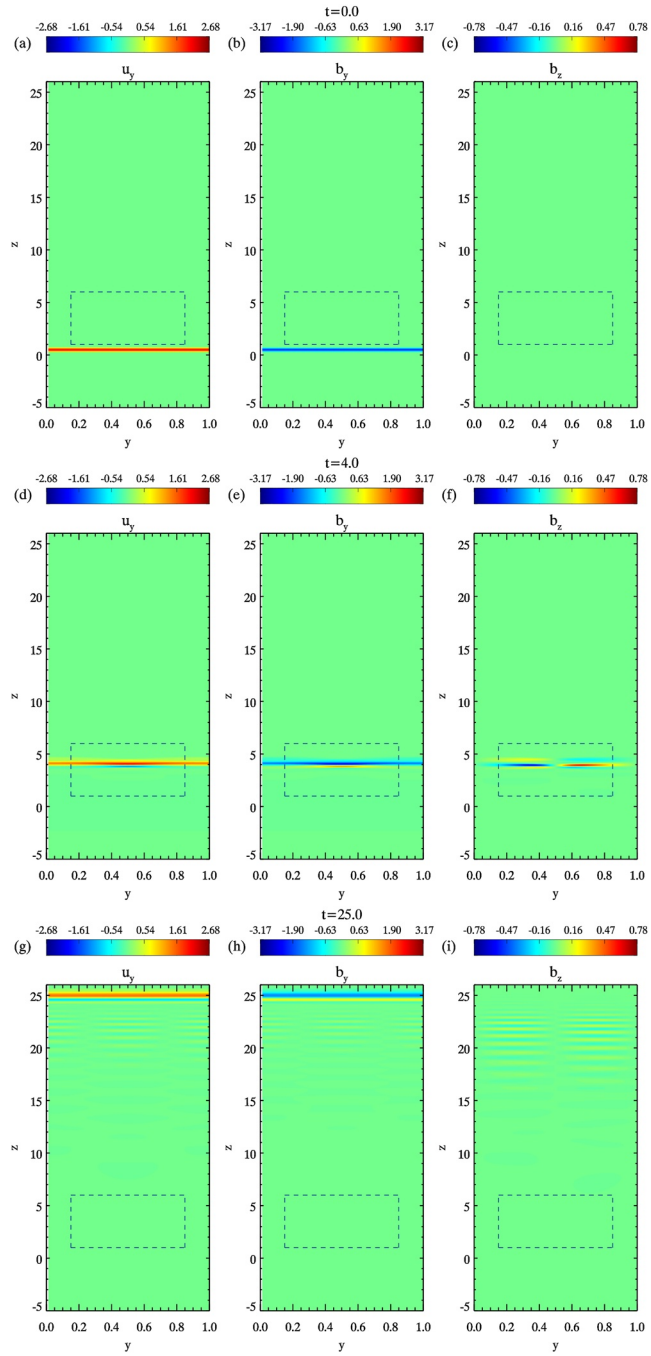

Figure 6. Contour plots of the simulation perturbations, $\Delta V = -0.3$. Each row of contour plots show u_y, b_y, and b_z at a particular time, for $\Delta V = -0.3$. The nonuniformity is marked on each panel by the dashed rectangle which marks the boundaries $y_a = 0.15$, $y_b = 0.85$, $z_a = 1$, $z_b = 6$. Panels (a–c) show the wave at $t = 0.0$. The wave is in the lower uniform region of the simulation, therefore, there has been no mode coupling, and there is no b_z. Panels (d–f) show the wave at $t = 4.0$, propagating through the nonuniform region (marked by the dashed rectangle), and the wave has mixed properties. There are clear contributions in b_z. Panels (g–i) show the wave at $t = 25.0$, the end of the simulation. The transmitted waves are now in the upper uniform region and the reflected waves in the lower. Evidence of both wave modes can be seen in panels (g and h). The parts of the wave that have propagated furthest $z > 24.5$ appear invariant in y are associated with the Alfvén wave. The waves that have a sinusoidal y variation (also visible in panel (i)) are compressional and come from the fast mode.

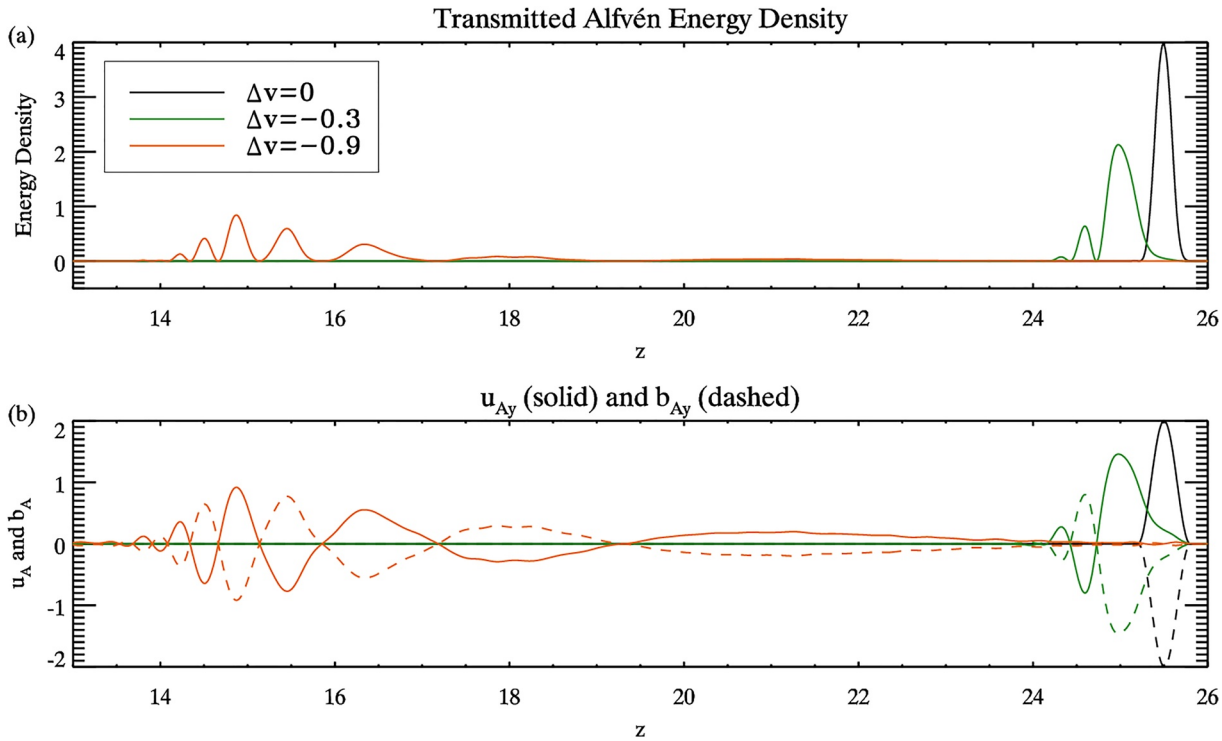

Figure 7. Transmitted Alfvén energy density (in z) and transmitted Alfvén wave perturbations, for $t = 25.0$, $\Delta V < 0$. Panel (a) shows the energy density in z of the transmitted Alfvén wave, $\mathcal{E}_A$ (see Equation 20), in the region $13 < z < 26$ at the simulation end time, $t = 25.0$. Panel (b) shows the Alfvén wave perturbations u_{Ay} and b_{Ay} which correspond to the lines in panel (a) and clearly satisfy $\rho^{1/2}u_y = -b_y$ ($\rho = 1$ for $z > 6$). Both panels show the slowing of the Alfvén wave when it has propagated through the decreased Alfvén speed region. In each case, this has lead to stretching of the Alfvén wave and the wave has developed multiple peaks and increased the width of the leading peak.

Figure 8 was created using 58 runs of the simulation for values of ΔV spanning -0.95 to 0, this range has been chosen as when $\Delta V = -0.96$, $T_p = 25.0$, this means that the wave does not have sufficient time to propagate through the nonuniform region. For each of these runs, data was collected at the simulation end time $t = 25.0$. The same definitions as the previous case (Section 3.1) are used such that transmitted energy is from the region $z > z_b = 6$, reflected energy is from $z < z_a = 1$, and trapped energy from $z_a = 1 < z < z_b = 6$.

Figure 8a shows the entire range, $-0.95 < \Delta V < 0$. As the medium becomes more nonuniform (ΔV becomes more negative) the transmitted Alfvén energy is seen to decrease slowly, while the transmitted fast energy slowly increases. The trapped energy is clearly negligible for the smaller ΔV cases, beginning to increase around $\Delta V = -0.6$.

Figures 8b and 8c show the larger and smaller quantities for a reduced range of ΔV, $-0.5 < \Delta V < 0$. It is interesting that the oscillatory behavior of the transmitted energy is seen again for both the Alfvén and fast wave modes. It is also interesting that reflection is not a major process in these interactions, with almost no reflected fast wave, and very little reflected Alfvén wave. As in the previous section, the oscillations in the energy are well resolved and are not numerical artifacts.

3.3. $\Delta V > 0$, Nonuniform Region Extended in z

In this section, the positive ΔV case ($\Delta V > 0$) is revisited; however, the nonuniform region is extended such that it is bounded by $z_a = 1$ and $z_b = 11$. The simulation run time is extended to 17.5 time units with the simulation bounded by $-17 < z < 28$. The results for this case will be compared to the results of the original $\Delta V > 0$ case (Section 3.1), to highlight the effect of extending the nonuniform region in z.

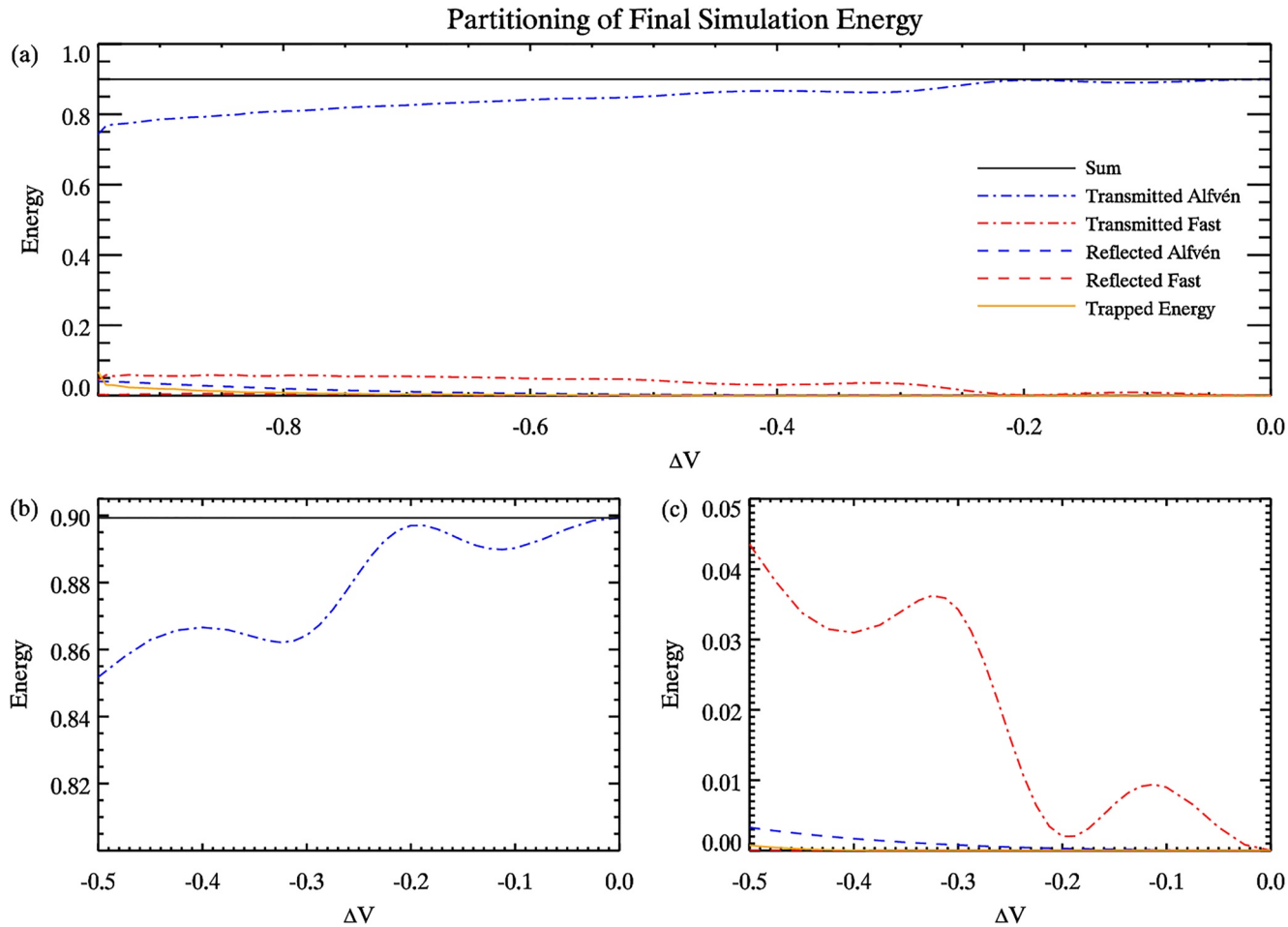

Figure 8. Partitioning of simulation energy between different waves. These plots show how the energy associated with the transmitted and reflected waves at the simulation end time changes with ΔV. All panels show the same data set. Panel (a) shows all wave categories for the range $-0.95 < \Delta V < 0$. It can be seen that Alfvén wave energy transmission decreases gradually as ΔV decreases. The trapped wave energy is clearly negligible where ΔV is small, as expected it increases as ΔV decreases. Panels (b and c) show large and small quantities separately. Interesting oscillatory behavior is seeing in both of the transmitted waves, but is not present in the reflections (similar behavior is seen in Figure 5).

Figure 9 is produced by decomposing the variables as described in Section 2.6, and integrating to find the energy densities in z (see Equations 16–21). In Figures 9a and 9b, the black line shows the $\Delta V = 0$ case, as there is no nonuniformity, the structure of the wave at the simulation end time is a translation of the initial condition by the simulation run time (17.5 time units). The green line shows the $\Delta V = 1$ case, it is clear that parts of the wave have traveled faster than in the $\Delta V = 0$ case, with the leading edge of the wave seen at $z = 19.6$. As in the previous sections, propagating through the nonuniformity causes the Alfvén wave to develop multiple peaks and broadens the spatial scale in z of the leading peak. The orange line shows the $\Delta V = 5$ case, with the leading edge of the wave now reaching $z = 20.8$, and breaking into a greater number of peaks.

Panel (c) of the figure shows the transmitted Alfvén wave at the end of the original (Section 3.1) and extended cases for $\Delta V = 5$. It shows that propagating through the extended nonuniform region causes the transmitted Alfvén wave to develop more peaks than in the original case. It is also clear that these peaks have reduced heights, interestingly, with more peaks, the distribution of energy density in z is more complex with the first and fourth peaks having a greater height than the second and third peaks.

Figure 10 shows the partitioning of energy between the waves at the end point of the simulation, for values of ΔV spanning 0–5, in order to investigate the relationship between the extent of the nonuniformity and the

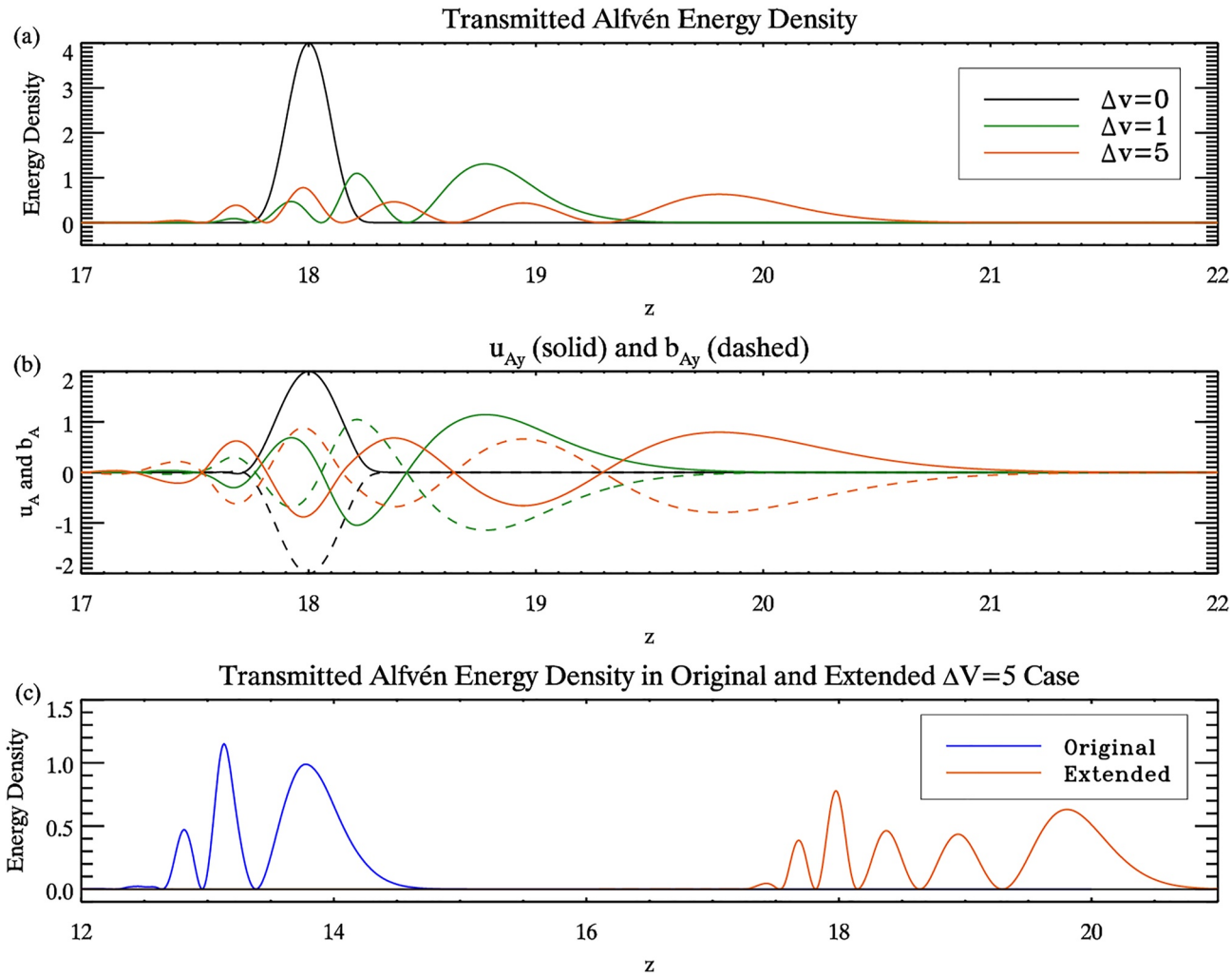

Figure 9. Transmitted Alfvén energy density (in z) and transmitted Alfvén wave perturbations, for $t = 17.5$, $\Delta V > 0$. Panel (a) shows the energy density in z of the transmitted Alfvén wave, $\mathcal{E}_A$ (see Equation 20), in the region $17 < z < 22$ at the simulation end time, $t = 17.5$. Panel (b) shows the Alfvén wave perturbations u_{Ay} and b_{Ay} which correspond to the lines in panel (a) and clearly satisfy $\rho^{1/2}u_y = -b_y$ ($\rho = 1$ for $z > 11$). Both panels show the increased propagation distance of the Alfvén wave when it has propagated through the increased Alfvén speed region. In each case, this has lead to stretching of the Alfvén wave and the wave has developed multiple peaks and increased the width of the leading peak. Panel (c) shows the transmitted Alfvén energy density in z at the end time of the original (Section 3.1) and extended (Section 3.3) cases for $\Delta V = 5$. It shows that in the extended case, the transmitted Alfvén wave develops more peaks than the original case and travels further.

oscillatory behavior of the transmitted waves in ΔV found in Section 3.1. As the nonuniform region has been expanded in z the upper boundary of the nonuniform region is now $z_b = 11$. This means that the definitions for reflected energies remains the same (energy from the region $z < z_a = 1$); however, the definitions for trapped and transmitted energy change. Trapped energy is now energy in the region $z_a = 1 < z < z_b = 11$, while transmitted energy is associated with parts of the wave that have propagated through the nonuniform region and into the upper uniform region $z > z_b = 11$. Panels (a) and (b) show the larger and smaller energies, respectively. The oscillatory behavior seen in Figure 5 is present again. It can also be seen that extending the nonuniform region, and therefore decreasing the gradient of the Alfvén speed in the nonuniform region, has lead to a decrease in both wave coupling and reflection even though the duration of the waves interaction with the nonuniform region has increased.

Panel (c) shows the transmitted fast energy against ΔV for the original $\Delta V > 0$ case (Section 3.1) and in the extended case (also plotted in panel (b)). Panel (d) shows the spatial scale of the transmitted fast wave oscillation in ΔV, which is denoted δV, this is calculated by finding the peak-to-peak and trough-to-trough distances and plotting them at the midpoint of the oscillation in ΔV. Interestingly, there is a clear correlation between the extent in z of

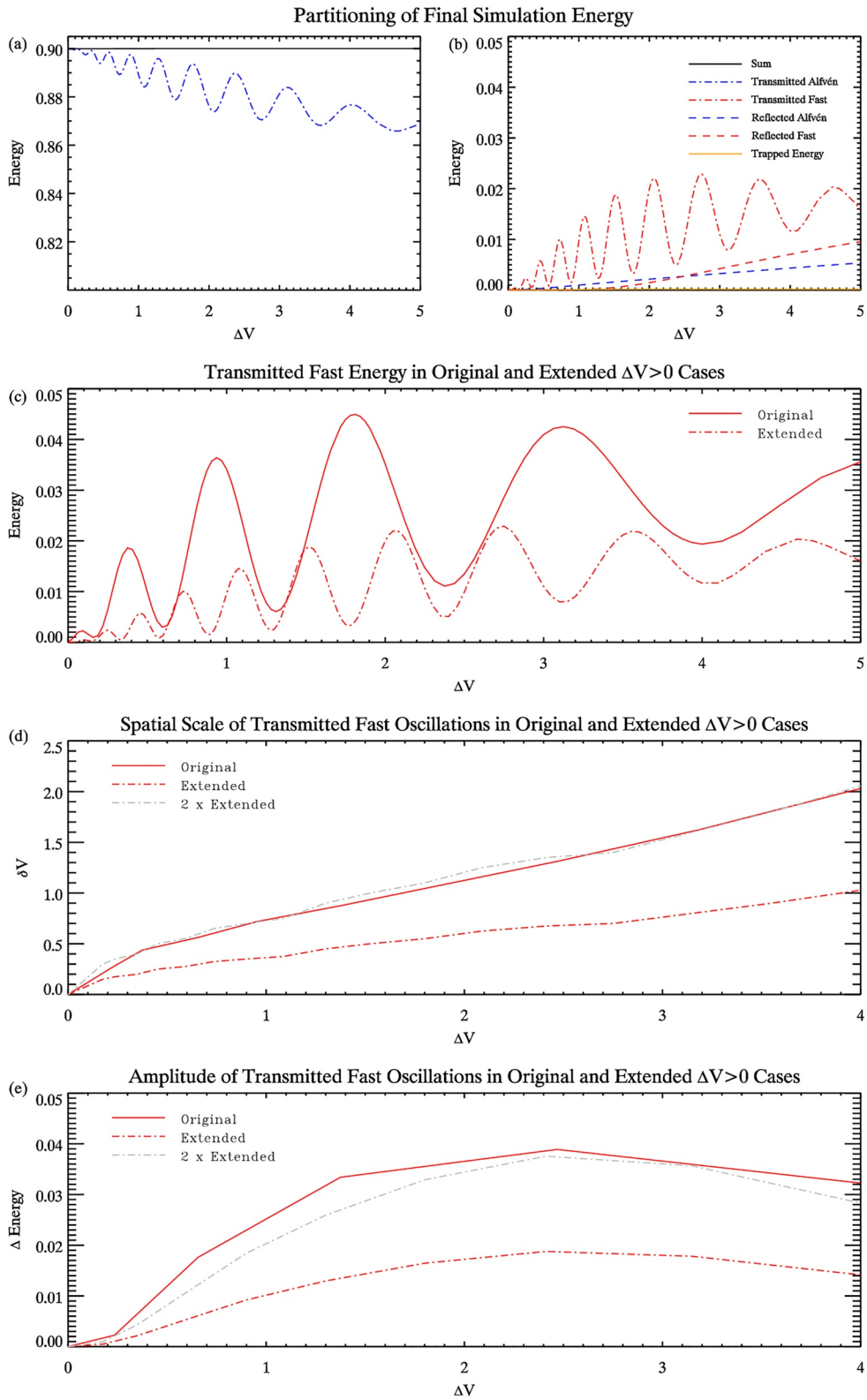

Figure 10.

the nonuniform region and the spatial scale of the oscillations of the transmitted energies. Doubling the extent of the nonuniformity causes the spatial scale of the oscillation to halve. In panel (c), this is shown by the dashed line of the extended case, which fits two cycles of the oscillation into one oscillation of the original case. In panel (d), this is shown by the gray dashed line, which is $2\delta V$ for the extended case, matching closely to the solid red line of δV for the original case.

Panel (e) shows that while the spatial scale of the oscillations clearly halves, this is not the case for the amplitude of the oscillations. The plot shows the amplitude of each oscillation, calculated as the trough-to-peak difference, against the midpoint of the trough and peak locations in ΔV for each case. The gray dashed lines shows two times the amplitude for the extended case, which is not a close but not exact match for the solid red line showing the amplitude of the original case.

4. Conclusion

This paper has investigated the propagation of Alfvén waves through a nonuniform medium in a low-beta, ideal plasma, using numerical simulation. By varying the magnitude, sign, and extent in z of the nonuniform Alfvén velocity profile, trends in the energy associated with the wave modes were observed.

The Alfvén wave displayed surprising efficiency in transmitting energy through the nonuniformity, although the wave structure becomes significantly distorted. The simulation results for the $\Delta V > 0$ case show energy transmission efficiency of 80% or better for the Alfvén wave energy, dependent on the magnitude of the nonuniformity, ΔV; with less than 8% of the total energy reflected by the nonuniformity as an Alfvén wave. Wave coupling was found to be far less efficient than anticipated, with a maximum of 12% energy conversion at the final time-step being associated with the fast mode. For the $\Delta V < 0$ case, broadly similar results are seen, with efficient transfer of Alfvén energy. In this regime, reflection of the wave off the nonuniformity is minimal and in contrast to the $\Delta V > 0$ case, accounts for significantly less energy than wave mode conversion. These results are consistent with observations of Alfvén waves which show they are able to maintain their identity well when propagating through nonuniform plasmas, for example, in the Jovian magnetosphere, there is strong Alfvén wave activity at the foot point of the Io-Jupiter flux tube which is present with decreasing intensity throughout the footprint tail (Gershman et al., 2019). Other simulations have shown Alfvén waves propagating with high efficiency in the magnetosphere through the formation of Alfvén ducts which guide the Alfvén wave along a flux tube (Yang et al., 2022).

Section 3.3 shows that the results of the earlier Sections 3.1 and 3.2, are not an isolated special case but are also observed where the extent of the nonuniform region differs. These results highlight the importance of the spatial extent of the nonuniform region.

The oscillatory behavior produced by plotting the transmitted Alfvén and fast energies against ΔV suggests that the interaction between a wave and a density gradient may be more complex than previously thought, with the results in Section 3.3 showing the clear correlation between the spatial scale of the oscillation and the extent in z of the nonuniform region. The scale of the Alfvén wave in z will be stretched (or compressed) when it encounters an increase (or decrease) in Alfvén speed, V. The scale of the wave compared to that of the V profile may lead to complex interference patterns in the transmitted Alfvén and fast waves, analogous to light reflecting off a thin film of oil. Further work on Alfvén-fast wave coupling is possible, including repeating this experiment for a three-dimensional flux tube, investigating the effect of a more complicated magnetic field geometry or for standing waves rather than distinct wave pulses.

Figure 10. Partitioning of simulation energy between different waves. These plots show how the energy associated with the transmitted and reflected waves at the simulation end time changes with ΔV, the vertical scales match Figure 5 to allow for easier comparison. Panels (a and b) show large and small quantities separately. Interesting oscillatory behavior is seen in both of the transmitted waves, but is not present in the reflections. The overall trend shows that Alfvén energy transmission decreases as ΔV increases, while fast wave coupling increases as ΔV increases, though they appear to be tending toward a constant value. Panel (c) shows the transmitted fast energy as a function of ΔV for both the original and extended $\Delta V > 0$ cases. It is clearly shown that doubling the extent in z of the nonuniform region has halved the spatial scale of the oscillations. Panel (d) also shows the spatial scale of the transmitted fast wave oscillations in ΔV by plotting the peak to peak and trough to trough distances δV against ΔV, with the gray line which shows $2\delta V$ for the extended case providing a good match for the standard case δV. Panel (e) shows that the amplitude of the oscillations in the extended case is approximately half of the amplitude in the original case.

Data Availability Statement

The data set used to produce the simulation figures in this paper is Davies (2023).

Acknowledgments
The authors acknowledge financial support by the UK's Science and Technology Facilities Council (STFC). R.D. was supported by STFC Doctoral Training Partnership Grant ST/T506436/1. A.N.W. was partially supported by STFC Grant ST/W001195/1.

References

Boocock, C., & Tsiklauri, D. (2022). Enhanced phase mixing of torsional Alfvén waves in stratified and divergent solar coronal structures–II. Non-linear simulations. *Monthly Notices of the Royal Astronomical Society*, *510*(2), 2618–2627. https://doi.org/10.1093/mnras/stab3592

Botha, G., Arber, T., Nakariakov, V., & Keenan, F. (2000). A developed stage of Alfvén wave phase mixing. *Astronomy & Astrophysics*, *363*(3), 1186–1194.

Bulanov, S., Shasharina, S., & Pegoraro, F. (1992). Transformation of MHD modes near magnetic separatrix surfaces. *Plasma Physics and Controlled Fusion*, *34*(1), 33–48. https://doi.org/10.1088/0741-3335/34/1/002

Cally, P. S., & Goossens, M. (2008). Three-dimensional MHD wave propagation and conversion to Alfvén waves near the solar surface. I. Direct numerical solution. In L. Gizon, P. Cally, & J. Leibacher (Eds.), *Helioseismology, asteroseismology, and MHD connections* (pp. 251–265). https://doi.org/10.1007/978-0-387-89482-9_19

Davies, R. (2023). Data for figures—Davies Wright, for submission to Earth and Space Science 2023. Retrieved from https://figshare.com/articles/dataset/Data_for_Figures_-_Davies_Wright_for_submission_to_JGR_Space_Physics_2023/21916689

Elsden, T., Wright, A., & Degeling, A. (2022). A review of the theory of 3-D Alfvén (field line) resonances. *Frontiers in Astronomy and Space Sciences*, *9*, 917817. https://doi.org/10.3389/fspas.2022.917817

Erdélyi, R. (2007). Magnetohydrodynamic waves. *AIP Conference Proceedings*, *919*, 122–137.

Gershman, D. J., Connerney, J. E. P., Kotsiaros, S., DiBraccio, G. A., Martos, Y. M., Viñas, A. F., et al. (2019). Alfvénic fluctuations associated with Jupiter's auroral emissions. *Geophysical Research Letters*, *46*(13), 7157–7165. https://doi.org/10.1029/2019gl082951

Goossens, M. L., Arregui, I., & Van Doorsselaere, T. (2019). Mixed properties of MHD waves in non-uniform plasmas. *Frontiers in Astronomy and Space Sciences*, *6*, 20. https://doi.org/10.3389/fspas.2019.00020

Grodent, D., Bonfond, B., Radioti, A., Gérard, J.-C., Jia, X., Nichols, J. D., & Clarke, J. T. (2009). Auroral footprint of Ganymede. *Journal of Geophysical Research: Space Physics*, *114*(A7), A07212. https://doi.org/10.1029/2009ja014289

Keiling, A. (2009). Alfvén waves and their roles in the dynamics of the Earth's magnetotail: A review. *Space Science Reviews*, *142*(1), 73–156. https://doi.org/10.1007/s11214-008-9463-8

McClements, K., Shah, N., & Thyagaraja, A. (2006). The coupling of shear and fast Alfvén waves at a magnetic x-point. *Journal of Plasma Physics*, *72*(4), 571–585. https://doi.org/10.1017/s0022377805004277

Mura, A., Adriani, A., Connerney, J. E. P., Bolton, S., Altieri, F., Bagenal, F., et al. (2018). Juno observations of spot structures and a split tail in Io-induced aurorae on Jupiter. *Science*, *361*(6404), 774–777. https://doi.org/10.1126/science.aat1450

Nakariakov, V. M., Pilipenko, V., Heilig, B., Jelínek, P., Karlický, M., Klimushkin, D. Y., et al. (2016). Magnetohydrodynamic oscillations in the solar corona and Earth's magnetosphere: Towards consolidated understanding. *Space Science Reviews*, *200*(1), 75–203. https://doi.org/10.1007/s11214-015-0233-0

Nakariakov, V. M., Roberts, B., & Murawski, K. (1997). Alfvén wave phase mixing as a source of fast magnetosonic waves. *Solar Physics*, *175*(1), 93–105. https://doi.org/10.1023/a:1004965725929

Ofman, L., Davila, J., & Steinolfson, R. (1994). Nonlinear studies of coronal heating by the resonant absorption of Alfvén waves. *Geophysical Research Letters*, *21*(20), 2259–2262. https://doi.org/10.1029/94gl01416

Pryor, W. R., Rymer, A. M., Mitchell, D. G., Hill, T. W., Young, D. T., Saur, J., et al. (2011). The auroral footprint of Enceladus on Saturn. *Nature*, *472*(7343), 331–333. https://doi.org/10.1038/nature09928

Rae, I., & Roberts, B. (1982). On MHD wave propagation in inhomogeneous plasmas and the mechanism of resonant absorption. *Monthly Notices of the Royal Astronomical Society*, *201*(4), 1171–1182. https://doi.org/10.1093/mnras/201.4.1171

Soler, R., Terradas, J., Oliver, R., & Ballester, J. L. (2017). Propagation of torsional Alfvén waves from the photosphere to the corona: Reflection, transmission, and heating in expanding flux tubes. *The Astrophysical Journal*, *840*(1), 20. https://doi.org/10.3847/1538-4357/aa6d7f

Southwood, D. (1974). Some features of field line resonances in the magnetosphere. *Planetary and Space Science*, *22*(3), 483–491. https://doi.org/10.1016/0032-0633(74)90078-6

Wright, A. N. (1987). The interaction of Io's Alfvén waves with the Jovian magnetosphere. *Journal of Geophysical Research: Space Physics*, *92*(A9), 9963–9970. https://doi.org/10.1029/ja092ia09p09963

Yang, Z., Zhang, B., Lotko, W., Sorathia, K. A., Pham, K., Luan, X., et al. (2022). Formation of Alfvén wave ducts by magnetotail flow bursts. *Journal of Geophysical Research: Space Physics*, *127*(9), e2022JA030841. https://doi.org/10.1029/2022ja030841

Yates, J. N., Southwood, D. J., Dougherty, M. K., Sulaiman, A. H., Masters, A., Cowley, S. W. H., et al. (2016). Saturn's quasiperiodic magneto-hydrodynamic waves. *Geophysical Research Letters*, *43*(21), 11–102. https://doi.org/10.1002/2016gl071069

Zalesak, S. T. (1979). Fully multidimensional flux-corrected transport algorithms for fluids. *Journal of Computational Physics*, *31*(3), 335–362. https://doi.org/10.1016/0021-9991(79)90051-2

Zheng, J., Chen, Y., & Yu, M. (2015). Nonlinear Alfvén wave propagating in ideal MHD plasmas. *Physica Scripta*, *91*(1), 015601. https://doi.org/10.1088/0031-8949/91/1/015601